PHOTOPTICS 2016, Selected and Extended Papers, Springer, 2017

Waveguide Evanescent Field Fluorescence and Scattering Microscopy: the status quo

Silvia Mittler
Department of Physics and Astronomy, The University of Western Ontario, London, Ontario, N6A 3K7, Canada
smittler@uwo.ca

Abstract

In the last years Waveguide Evanescent Filed Fluorescence (WEFF) and Scattering (WEFS) microscopy were developed which are alternatives to TIR and TIRF microscopy. Both technologies implement a slab waveguide-microscopy chip with a coupling grating. The technologies are described and compared to TIR and TIRF microscopy. The advantages of the waveguide method are clearly addressed. A brief history of the technology's development and similar activities in the field are discussed. Application examples from both WEF microscopies follow: static distance mapping with a multimode waveguide, dynamic solubilisation studies of cell plasma membranes and the kinetic response of osteoblasts to trypsin (WEFF); bacteria sterilization as well as cell adhesion and granularity studies (WEFS). The combination of both methods is discussed and found not suitable. In order to mass fabricate the necessary waveguide chips with the grating an all-polymer-waveguide chip was developed. This should allow to bring the new microscopy methods to the interested scientific community.

1. Introduction

With the aim of developing new medical devices with direct tissue contact, drug delivery vehicles, and tissue engineering scaffolds, there has been increasing interest in recent years in the interactions of cells with both synthetic and natural biomaterials (Niu et al. 2005; Storrie et al. 2007). In particular, the study of the contact regions between a cell and its substratum is of considerable interest as its investigation delivers *inter alia* information about the cytocompatibility of the substratum - the affinity of cells towards that particular surface. Promotion or inhibition of cell adhesion to synthetic and natural biomaterials is often crucial to the proper function of a particular device. Some information concerning these interactions, e.g. the lateral location and the density of the adhesion sites, as well as their relationship to the actin stress fiber system, part of the cell's cytoskeleton, can be inferred from fluorescence microscopy of immunolabeled molecules involved in adhesion; typically, vinculin, a protein located within the multi-protein complex that anchors the adhesion to the cytoskeleton inside the cell (Burmeister et al. 1998). These methods

only deliver signals from the focus volume and no information about adhesion distances to the substratum. However, a direct and quantitative method to address the distance to the substratum is highly attractive. To address this need, different microscopic techniques based on electron microscopy (Chen and Singer 1982) and optical means such as evanescent fields and interference techniques have been developed. Total internal reflection fluorescence (TIRF) (Burmeister et al. 1998; Burmeister et al., 1994), surface plasmon resonance microscopy (SPRM) (Giebel et al. 1999), interference fluorescence microscopy (IRM) (Verschueren 1985), fluorescence interference contrast (FLIC) microscopy (Braun, 1997) and combinations thereof (Burmeister et al. 1998; Atilgan and Ovryn 2009) have been used to visualize and quantify these contacts. The contacts themselves had been discovered by interference reflection microscopy (IRM) in the 1970s (Abercrombie et al. 1971).

Bacteria, on the other hand, are the most metabolically diverse group of organisms found in all natural environments including air, water and soil. Bacteria commonly occur with food sources and are also found within and on our bodies. However, concerns exist over contamination of food, water, and air by pathogenic bacteria (Sapsford and Shiver-Lake 2008) that can enter our bodies through ingestion, inhalation, cuts or lacerations (Pizarro-Cerda and Cossart 2006). Therefore, there is an increasing interest in bacterial contamination and the need for anti-bacterial surfaces not only for application in the food industry but also for medical and hygienic purposes (Oliver 2005). Over two million hospital-acquired cases of infection are reported annually in the USA, which lead to approximately 100,000 deaths annually and added nearly $5 billion to U.S. healthcare costs (Madkour and Tew 2008; Madkour et al. 2009). Contamination of medical devices (e.g., catheters and implants) has been attributed to 45% of these infections (Stamm 1978). Bacterial contamination of any surface typically begins with the initial adhesion of only a few cells that can then develop into a more structurally cohesive biofilm in less than 24 hours when provided with suitable nutrient conditions sustaining metabolism and cell division (Hetrick and Schoenfisch 2006). Therefore, a better understanding of bacterial adhesion to surfaces is important for technical surface development and in biomedical applications. However, the precise measurement of bacterial adhesion to surfaces are difficult and time consuming because bacterial cells typically occur on the micrometer-scale and their adhesion forces are generally low, typically 0.1–100 nN (Christianson 2004). Recent studies on the detection of bacteria on surfaces have focused on similar imaging systems as with cells such as optical (Vasilev et al. 2009) and fluorescent microscopy (Pires et al. 2013) to image the bacteria themselves or luminescence measurement of the presence of cells by ATP (adenosine triphosphate) detection systems (Pera et al. 2010). Surface Plasmon Resonance (SPR) sensors (Taylor et al. 2008), Nucleic Acid Detection (Schmidt et al. 2006), Optical Waveguide Lightmode Spectroscopy (short: waveguide spectroscopy) (Cooper et al. 2009), Optical Leaky Waveguide Sensors (Zourob et al. 2005), and Evanescent Mode Fiber Optic Sensors (Mazhorova et al. 2012) have also been applied in order to detect biochemical toxins as signatures of bacteria.

In conclusion, it is important to have methods available which are able to investigate interfaces between a technical surface and a bacterium or cell.

In recent years, Total Internal Reflection Fluorescent (TIRF) microscopy has been demonstrated to be an effective method for studying cell-substrate interactions that occur at surfaces and interfaces. Using TIRF microscopy, the behavior of various types of cells (Bauereiss et al. 2015; Liu et al. 2015) and bacteria (Smith et al. 2002, Vigeant et al. 2001) near surfaces has been characterized. Total Internal Reflection (TIR) Microscopy utilizes the basic technology of TIRF without any fluorescence dyes present in the sample by creating an optical contrast due to

scattering (Byrne et al. 2008). Recent studies have also demonstrated the use of TIR for imaging microbial adhesion.

This paper will give a brief history and literature overview as well as a review on biophysical applications of WEFF and WEFS microscopy on cells and bacteria and a short outlook on current developments on mass producible all-polymer-waveguide-chips to offer the methods to a broader user base.

2. Brief History

The waveguide evanescent field scattering (WEFS) technique was developed by Thoma et al. in 1997 [Thoma et al. 1997; Thoma et al. 1998) for ultrathin technical structures on surfaces using conventional ion exchanged waveguides. Thoma et al. investigated the influence of the polarization direction of the mode and the mode number on the achieved scattering image contrast. It was found that with increasing mode number the contrast increased. TE modes depicted a better contrast than TM modes. Immersion of the samples in an aqueous solution decreased the contrast as the refractive index difference between scattering centers and the surrounding medium decreased.

Before the first cells were imaged evanescently with a waveguide, a series of approaches were made to combine established microscopy methods with a conventional waveguide and waveguide spectroscopy to on-line monitor e.g. adhesion and proliferation of cultured cells (Hug et al. 2001; Hug et al. 2002a/b). These attempts suffered from the small penetration depth of the evanescent fields into the cells of the used conventional waveguides. Therefore, Horvath et al. proposed in 2005 reverse symmetry waveguides which provided deeper penetrating evanescent fields in these combination technologies.

The first waveguide evanescent field fluorescence (WEFF) experiment with commercial mono-mode glass waveguides (designed for sensing on coupling gratings) on cells was shown by Gradin et al. (Gradin et al. 2006). Vinculin staining was carried out on fixed human fibroblast cells. The coupling was carried out via a coupling grating located within the sample area. The image suffered from substantial artefacts and was very noisy in form of stripes. The position of the grating in the field of view lead to too many scattered photons and to resonantly out-coupled light.

WEFF microscopy with ion exchanged mono- or multi-mode glass waveguides and stained cell's plasma membranes was developed by Hassanzadeh et al. in 2008 (Hassanzadeh et al. 2008) as a straightforward alternative to TIRF microscopy for imaging ultrathin films and cell-substrate interaction. The mode coupling was achieved via a grating coupler outside the imaging area. The image quality was increasing, but artefacts due to scattered light were still seen in the images and are not completely avaoidable. TIRF images share the same issues (Hassanzadeh et al. 2010). Hassanzahdeh et al. have then shown applications of WEFF microscopy with static and dynamic investigations (Hassanzadeh et al. 2008, Hassanzadeh and Mittler 2011, Hassanzadeh et al. 2012). They were the first who used a multi-mode waveguides with mode selective grating coupling to detremine distances of cell adhesions to the waveguide surface (Hassanzadeh et al. 2009).

A year later, 2009, Agnarsson et al. (Agnarsson et al. 2009) presented a symmetric waveguide structure for WEFF microscopy where the cladding material is index-matched to the sample solution (aqueous media). The optical chips were fabricated from polymers involving standard cleanroom technologies such as spin-coating, photolithography and dry etching (core:

polymethylmethacrylate (PMMA) and substrate: amorphous perfluorinated optical polymer (Cytop)). Agnarsson et al. coupled via end-fire coupling mode-insensitive into a mono-mode waveguide. MCF7 breast cancer cells immune-stained with monoclonal antibody against the transmembrane adhesion protein E-cadherin (HECD-1) and Alexa Fluor 546 Goat Anti Mouse IgG1 fluorescent secondary antibody. Very clear WEFF images were obtained with some minor scattering artefacts. Agnarsson et al. were combining WEFF microscopy on the mono-mode polymer symmetric waveguide structures with waveguide spectroscopy and channel waveguide operation (directional couplers, ring resonators, Mach-Zehnder interferometers, etc.) for sensing application and on-chip control of illumination with sub-millisecond control (Agnarsson et al. 2010; Keshmiri et al. 2011; Arnasson et al. 2011; Leosson and Agnarsson 2012).

In 2014, Nahar et al. (Nahar et al. 2014) implemented WEFS microscopy for bacteria studies and started to investigate cultured ostoeblasts with WEFS microscopy.

Agnarsson et al. (Agnarsson et al. 2015) picked up WEFS microscopy in 2015 for label-free sensing of gold nanoparticles (AuNPs), vesicles and living cells, and compared it with WEFF results, all on symmetric polymer waveguide structures.

The focus of the following are the WEFF and WEFS studies of the author's group.

3. Experimental

3.1. Waveguides

In this study home-fabricated, glass waveguides on fused silica (step-index slab waveguides) or ion exchanged waveguides with holographic coupling gratings were used (Hassanzadeh, 2011; Halfpap, 2012). The waveguides were reusable various times after thorough cleaning. A typical cleaning procedure consisted of a submersion in 70 % ethanol (Aldrich, Canada) with sonication (Branson 2510, Branson, USA) for 20 min and a blow-dry with nitrogen gas. To remove organic material, the dried samples were cleaned with Nano-Strip (KMG Chemicals Inc., Fremont, CA, USA) at 80° C for 5 min. After the Nano-Strip application, the substrata were rinsed extensively in Milli-Q water and blown dry again. However, with each cleaning cycle the waveguides became thinner and needed characterization before every new experiment.

The samples were designed in a way that the coupling grating is always kept outside the sample area and should not be altered during the experiment to keep the coupling conditions and therefore, the coupling efficiency, constant. This is important because the mode coupling conditions change when material is adsorbed or desorbed at the grating position (Horvath et al. 2001). In addition, out-coupled photons from the grating produces artefacts in the WEFF and WEFS images. Any periodic structures should be avoided in the sample area due to undesired interference effects.

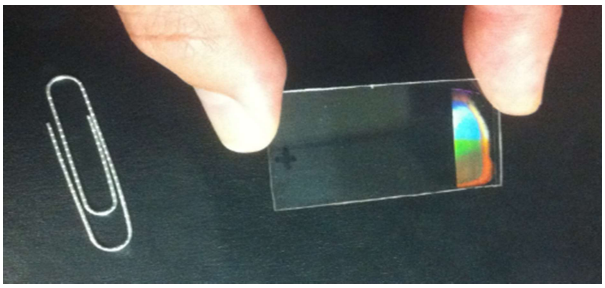

Fig.1 General WEFF- and WEFS chip design: the coupling grating is located outside the sample area.

3.2. Cell Culture

The osteoblastic cell line MC3T3-E1 (subclone 4, ATTC Catalog 3 CRL-2593) were cultured in flasks. The cleaned waveguides were sterilized for 3 h by UV light. Growth medium was prepared from 17.8 ml α-minimum essential medium 1X (MEM; Gibco), 2 ml fetal bovine serum (FBS; Gibco) and 0.2 ml antibiotic-antimycotic solution 100X (Anti-Anti; Gibco). First the medium was aspirated from the cell culture flask. Dulbecco's phosphate-buffered saline 1X (PBS; Gibco) was added to wash the cell layer and aspirated subsequently. To detach the osteoblasts from the vessel, wall, 5 ml trypsin-EDTA (0.05%, Gibco) was added and incubated at 37° C for 5 min. The culture was checked by phase-contrast microscopy to confirm that cells were released into the suspension. The trypsin was neutralized by adding 9 ml growth medium to the flask. The resulting cell suspension was diluted in growth medium to 10,000 cells per ml. Waveguides were placed in a Petri dish and 1 ml cell suspension per substrate was applied to the surfaces. Samples were then incubated for 24 h at 37° C, 100 % humidity and 5 % CO_2.

The waveguides were removed from the growth medium and excess medium was aspirated. Next, each waveguide was rinsed three times in PBS. For fixation, the waveguides with the cells on top were placed in a solution of 4 % paraformaldehyde in PBS for 10 min at room temperature. Subsequently, samples were rinsed three times with PBS. To prevent desiccation, samples were kept in PBS until further treatment. A solution was prepared from 1.5 mg DiO in 1 ml dimethyl sulfoxide (DMSO) and heated to 37° C within 5 min. This mixture was sedimented for 5 min at 2000 rpm to separate solid residues. 10 µl of this stock solution was dissolved in 1 ml growth medium to form the staining solution. The staining solution (200 µl) was pipetted onto the corner of each waveguide and the waveguide gently agitated until all cells were covered with staining solution. The samples were left in the solution for 20 min to incorporate the dye. Afterwards, the staining solution was drained and the waveguides were washed in PBS. For the removal of all unbound dye, the samples were immersed in PBS for 10 min and drained again. The entire wash cycle was repeated two more times. The waveguides were stored in PBS until performing WEFF microscopy. This procedure delivers fixed cells, cells that are "frozen" in their habitus (Lanier and Warner 1981; Smit et al. 1974; Su et al. 2014) with the dye situated in the plasma membrane of the cells.

3.3. Bacterial Culture

Nitrobacter sp. 263 was cultured on R2A (Difco™) plates at room temperature (approximately 23° C) for two weeks. For each colonization experiment, bacteria from one R2A plate were removed and suspended in 1 ml of filter-sterilized (0.45 µm pore-size) distilled deionized water to produce an aqueous bacterial suspension (with 10^6 bacteria/ml). A separate stock solution of R2B (i.e., broth/liquid culture medium) was made by dissolving R2A in sterile, distilled, deionized water and filtering this solution to remove the agar constituent leaving the dissolved nutrients for bacterial growth.

Bacterial attachment to the waveguide surface was achieved by placing a 50 µl aliquot of the bacterial suspension on top of the waveguide for one h at 37° C. After bacteria attached to the surface, the waveguide was rinsed with sterile, distilled water and placed in a sterile Petri dish containing 20 ml of R2A and incubated for 24 h at 37° to allow the attached bacteria to grow. The samples were not agitated. After 24 h incubation, the waveguides were examined using bright field microscopy to determine whether microcolonies had formed. All images were taken of live cells in growth medium. Samples were then analyzed using WEFS microscopy.

Sterilization experiments were performed. Separate bacteria suspensions of 10 ml (with 10^6 bacteria/ml) were placed in a sterile, open glass dish and exposed in a low pressure collimate beam apparatus (LPCB) to induce sterilization (Hedrick et al. 2007; Kuo et al. 2003) at doses of 2, 4, 8, 14, 20 and 30 mJ/cm^2 by increasing time to produce different doses (Kuo et al. 2003). This mode of UV photon sterilization was chosen for its common use in industrial applications and its ability to disrupt and dimerize neighboring DNA bases (thymine dimerization) that hinders bacterial growth but not viability (Berney et al. 2007; Durbeej and Eriksson 2002). Each 'sterilized' bacterial suspension, produced via the different dose exposures, was used in an identical colonization experiments as described above.

Prior to the first and second colonization experiment, separate aliquots of all bacterial suspensions (1ml) were stained using BacLight^{TM} (Invitrogen) Live-Dead stain and examined using fluorescence microscopy to confirm that the cells were viable.

3.4. WEFF and WEFS Microscope

The WEFF and WEFS microscope (Hassanzadeh et al. 2008, Sharon and Mittler 2016) consisted of an inverted microscope (Zeiss, Oberkochen, Germany) with the waveguide being located on the sample stage (Fig.2 and 3). The specimen was positioned on top of the waveguide. An argon ion laser (35 LAP 341-200, CVI Melles Griot) operated at λ = 488 nm with a variable output power of 7- 126 mW or a HeNe laser with a wavelength of 543.8 nm (Research Electro-Optics, 0.5 mW) were used as light sources in WEFF and WEFS microscopy, respectively. A neutral density filter was placed directly behind the laser for power reduction, avoiding bleaching and overexposure. An iris aperture controlled the beam diameter. The laser beam was coupled into a chosen waveguide mode by a coupling grating located on the waveguide. In the case of WEFF microscopy, the undesired excitation wavelength was blocked with a long pass filter with a cut-off wavelength of $\lambda_{cut\text{-}off}$ = 490 nm (3RD490LP, Omega Optics, Brattleboro, VT) which was fitted between the objective and the camera. The out-coupled intensity at the end of the waveguide was captured with a large active area photodiode (FDS1010, Thorlabs, Newton, NY) for determining the coupling efficiency when needed. A cooled CCD-camera (Persuit - XS 1.4 Diagnostic Instruments Inc., Sterling Heights, MI, USA), controlled with SPOT 5 Basic (Spot Image Solutions, Sterling Heights, MI, USA) was connected to a computer. Image data were exported for processing. Additionally, bright field microscopy images of the samples were captured with the same field of view/objective lens as the WEFF/WEFS microscopy images and processed with Image Pro Express (Media Cybernetics, Rockville, MD).

The coupling of the laser beam can be conducted either from below the waveguide chip in parallel to the objective lens as depicted in Fig.2. This has the advantage that all beam steering can be done on the optical table. The disadvantage is the close proximity to the objective lens which restricts the available coupling angle substantially and forbids backward coupling.

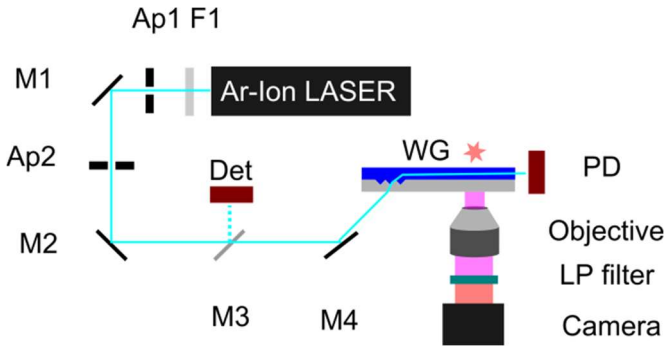

Figure 2: Schematic of WEFF microscope with coupling through the waveguide chip from below. Ap: aperture, F1: neutral density filter, M: mirror, WG: waveguide, PD: photo diode. For WEFS microscopy a HeNe laser was used and the LP filter omitted.

In the alternative design the coupling is carried out from the top (Fig.3). The advantage here is a restriction less coupling angle. The disadvantages are the possible reflections and scattered photons from the objective lens, and some of the beam steering needs to be carried out above the optical table making the system more prone to vibration issues.

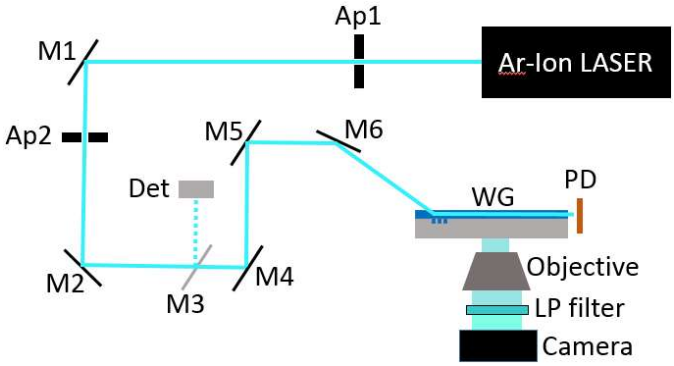

Figure 3: Schematic of a WEFS microscope with coupling into the waveguide from above. Ap: aperture, M: mirror, WG: waveguide, PD: photo diode. For WEFS microscopy a HeNe laser was used and the LP filter omitted. Optical elements Ap1 to M4 are mounted on the table.

4. TIRF/TIR and WEFF/WEFS Comparison

Both microscopy suits, TIRF/TIR and WEFF/WEFS, employ evanescent fields for sample illumination at the surface of a substrate which are produced by total internal reflection. In modern TIRF/TIR microscopes a laser beam is guided opto-mechanically within the microscope and the objective lens to allow a laser beam to undergo total internal reflection at a high refractive index substrate which carries the specimen and is located above the objective lens. Costly state-of-the

art equipment and objective lenses with specially designed high magnification and high numerical aperture objectives and built-in optical path control are necessary. Theoretically, all angles above the critical angle of TIR can be achieved in this way, giving the possibility to achieve different penetrations depth with different angles. This can be used to measure distances from the substrate surface (Truskey et al. 1992). Practically, the microscopes are set to particular angles, typically to receive a high quality TIRF or TIR image and a high quality epi-fluorescence or bright field image, respectively, taken with a transmitting beam.

On the other hand, operating a TIRF/TIR microscope manually can easily lead to a loss of the evanescent mode and to a full specimen exposure to the laser beam resulting in a damaged sample.

Reviewing the literature and in particular the use of TIRF microscopy for distance measurements shows that besides Burmeister's excellent work in the middle of the 1990s (Burmeister et al. 1994) during the development phase of TIRF microscopy only little has been published on exploiting different penetration depths.

TIR microscopy is performed identically but excluding the dye from the samples and the necessary filter sets. Scattered photons instead of fluorescence photons are collected. Bright field images are taken for comparison since epi-fluorescence is not possible. Little distance work has been published involving TIR microscopy (Smith et al. 2002). This is not surprising since the scattering intensities are hard to analyze because all refractive index fluctuations present in the evanescent field contribute to the signal and these are not necessarily controllable, in particular with living cultures producing extracellular matrix in the case of cells or extracellular polymeric substance (EPS) when imaging live bacteria.

In WEFF/WEFS microscopy the resonances of the waveguide modes dictate the available evanescent fields and penetration depths. So the number of choices is limited by the number of modes propagating in the waveguide. In TIRF and TIR microscopy, the penetration depth of the evanescent field is limited to a maximum of ~ 200 nm, whereas a waveguide can produce penetrations depths from below 100 nm to over a μm by tuning the refractive index and thickness architecture of the core and cladding layers (Agnarsson, 2009). Planar waveguides also offer an extended illumination area over macroscopic dimensions only limited by the attenuation of the propagating waveguide mode.

In addition, the beam in WEFF/WEFS can never escape the waveguide; therefore, WEFF and WEFS microscopies carry the intrinsic safety mechanism of avoidance of sample overexposure and damage.

In well characterized waveguides the evanescent fields and penetration depth are well known quantities and can be used for quantitative measurements (Hassanzadeh et al. 2009).

WEFF and WEFS microscopy do not desire state-of-the-art microscopes or objective lenses. WEFF and WEFS technologies are based on a few simple accessories and attachments to a standard inverted microscope. It is therefore straightforward to image the specimen in any magnification and field of view available due to standard long distance objective lenses by just turning the objective lens revolver without the necessity of beam stirring. Due to the evanescent field formation being taken care of by the substrate and completely independent from the entire microscope, different field of views or magnifications still deal with the same illumination conditions allowing direct comparison of images or measurements after changing magnification and field of view.

Epi-fluorescence images can be achieved by simply enhancing the integration time of image acquisition. This is due to non-perfect waveguides: every waveguide scatters slightly and therefore supplies the 3D volume of the specimen with excitation or scattering photons.

Comparing TIRF and WEFF images of the same samples has shown identical image information (Hassanzadeh et al. 2010). Both microscopy technology suits are diffraction limited, therefore the lateral resolution depends on the chosen laser wavelength and the highest possible magnification lens and its numerical aperture (NA) supported by the microscope used. The resolution in z-direction (perpendicular to the substrate) lies in both types of microscopes in the order of ~7 nm.

To achieve a wide use of WEFF and WEFS microscopy in the interested research communities it is necessary to have easy access to and supply of inexpensive waveguide substrates. Therefore, it is necessary to develop a mass producible waveguide-chip.

5. Static Distance Mapping with a Multimode Waveguide

A waveguide with a thickness of 651 ± 2 nm and a refractive index of n = 1.840 ± 0.001 was used for mapping the distances of the dye located in the plasma membrane of fixed osteoblasts. The volume above the waveguide was assumed to be water with a refractive index of 1.33 for simulating the evanescent fields. Two images taken with the TM_1 and TM_2 mode were used to calculate the dye distance map (Fleissner et al. 2014).

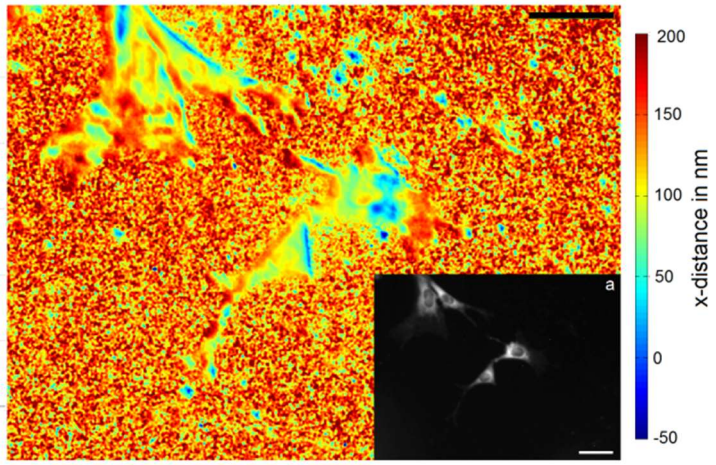

Figure 4: False color representation of a dye distance map with four osteoblasts. The inset represents a WEFF image with increased integration time of the same field of view. Both scale bars represent 50 µm.

The WEFF image in Fig.4 depicts four osteoblasts well spread and indicating the nuclei and some cell extensions. The dye distance map depicts lower distance-colors (blue to yellow) in the area of the cells from close to 0 to ~ 130 nm. In the unoccupied area, the unstained medium, where the raw data do not show fluorescence intensities, only noise is present. This is depicted as distances in the order of the penetration depth of the evanescent field: ~160 ± 40 nm (red pixels with yellow). In addition, isolated spots in the no-sample area (outside the cells) are visible in very dark blue. These spots are correlated to un-physical distance values below zero caused by microscopic damages of the waveguide. These un-physical distances should always be omitted in image interpretation. All four osteoblasts can be found in the distance map and show cell outlines

similar to the cells depicted in the "epi-fluorescence" image. However, the filopodia and the thinly spread cell body are even clearer in the distance map. In Fig.4, the distance map does not depict any information about the nuclei. Not the entire cell body reached down very close to the surface, as expected. At some of the cells' outer lines and at some extreme tips of the spread cells, small regions – only a few pixels in diameter – were found with distances of ~10 - 25 nm, typical of a focal adhesion (Chen and Singer 1982; Tavil et al. 1993). Twice line like accumulations of dense focal adhesions are found (blue lines with distances around 10 - 25 nm). Between the focal adhesions, there are regions in lighter blue depicting distances around 40 -50 nm as well as greenish areas depicting distances around 70 - 80 nm. Filopodia of the cells, which are very faintly seen in the epi-fluorescence images, are clearly visible in the distance map as thin spikes with a blue (possible focal adhesions or point contacts) or green (possible extracellular matrix contacts) center and green-yellow surroundings (Chen and Singer 1982).

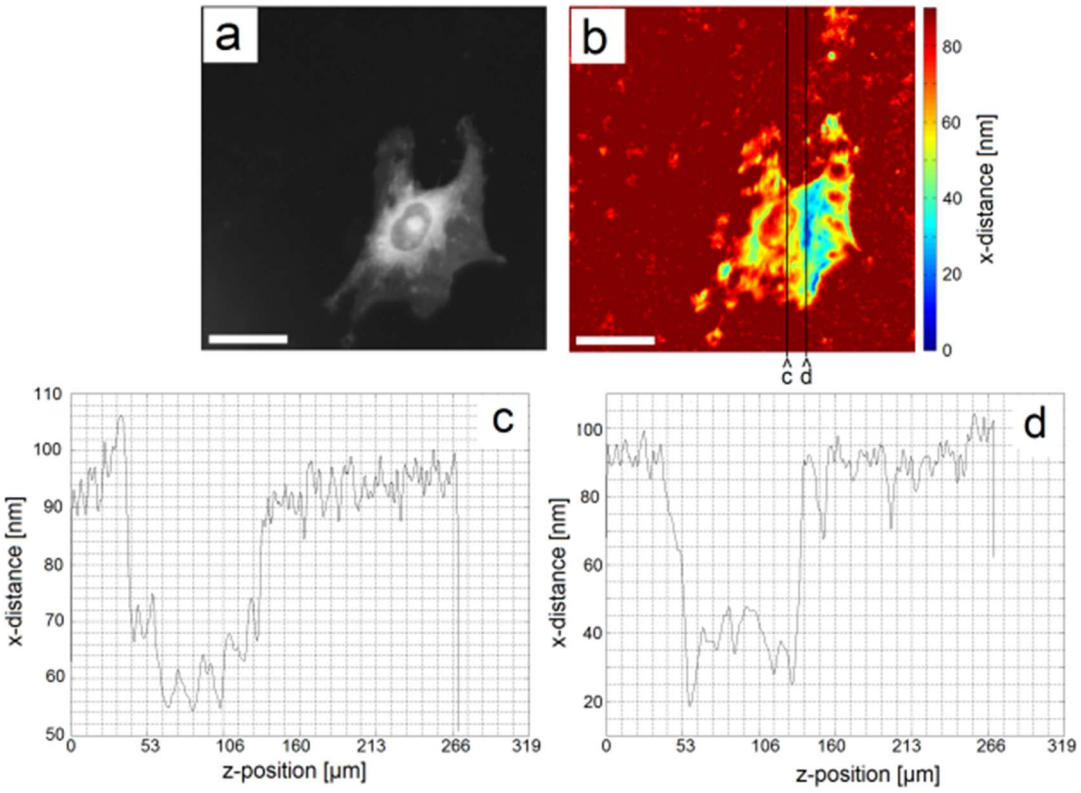

Figure 5: Single osteoblast. a) epi-fluorescence WEFF image, b) false color representation of the dye distance map, c) z-cut through cell at random position 'c' in part b) and d) z-cut through cell at smallest distance locations at position 'd' in b). The cuts in b) from bottom to top are represented in c) and d) from left to right. The scale bars represent 25 µm.

Fig.5 depicts one well spread osteoblast taken in epi-fluorescence WEFF mode and false color distance map. Two z-cuts through the distance map have been made: one randomly through the cell, (Fig.5c) and one through an area including the smallest distances of the cell (Fig.5d). The area outside the cell is nearly homogeneously dark red colored. The existing noise level in the no-sample regions is clearly depicted in the z-cut data; it is the noisy data at an average distance of ~ 90 nm on both sides of the cell. The cell itself is shown by the depressions in the z-cuts with the dips indicating adhesions. The spreading of the cell is excellently depicted by the distance map.

The cell is attached at all extreme spreading points, however not necessarily as focal adhesions since, distances above 40 nm and up to 50 nm, possible close contacts, are found. In the center of the cell, focal adhesions are present.

The z-cuts show the position of the plasma membrane/dye location along the cut line in nm. For the random cut 'c', three "small" distances in the order of ~ 55 nm are found, as well as a couple of more bends towards the substratum with distances of ~ 62 - 67 nm. The maximum heights of the plasma membrane from the waveguide surfaces between the bends towards the substratum are found to be between 62 and 75 nm.

In the z-cut 'd' through the small distance adhesions one focal adhesion at 18 nm is found as well as contacts with distances of 25 – 35 nm. The maximum heights of the plasma membrane from the waveguide surfaces in this case are 37 and 45 nm. The bending of the membrane towards the cytoplasm between these adhesions points is clearly depicted. The relative straight lines between the "maxima and minima" in the distance curve bear a resemblance to a stretched rubber band. One needs to keep in mind that the surface tension of the plasma membrane tries to minimize the surface area, trying to force the cell into a spherical shape. The adhesions are obvious biological disruptions of the physical effect of surface minimization.

It would be interesting to monitor and quantitatively analyze the dynamics of a living cell moving and forming lamellipodia and new adhesions as well as retrieving lamellipodia and withdraw adhesion. With the current set-up, time laps distance mapping it is not yet possible. An automated, motorized mirror adjustment for M4 (Fig.2) with a feedback loop for optimized coupling from the photodiode PD (Fig.2) needs to be implemented.

6. Dynamic Solubilisation Studies of Cell Plasma Membranes

Detergent-membrane interactions have been the subject of many studies (Ngassam et al. 2012). Functional membranes typically exist in the fluid state, also called the liquid-disordered state. Due to difficulties of working with authentic cell membranes, simplified membrane models - such as supported lipid bilayers or liposome mimicking biological systems - have often been used to investigate detergent-membrane interactions (Ngassam et al. 2012). Model membranes were helpful in exploring the basic membrane functions. However, in comparison to a living cell, with integral and peripheral proteins, cholesterol molecules and oligosaccharides in and on their plasma membrane, artificial membrane models cannot mimic all aspects of plasma membrane function. In addition, studying the interaction between lipids and detergents in the form of vesicles (liposomes) or supported lipid bilayers has several other disadvantages. For example, in supported lipid bilayers, the quality of the deposited film plays a major role. The direct contact with the underlying substrate affects the bilayer's structure and fluidity, and blocks access of solutions to both sides of the membrane.

The results of lipid-detergent interaction studies using bio-membrane models have been related to a three-stage model, which was described by Lichtenberg et al. (Lichtenberg et al. 1985). In stage I, with increasing detergent concentration, detergent incorporates into the bilayer. At this stage, solubilization does not occur, but the bilayer becomes saturated with detergent. At stage II, with further increase in detergent concentration, the bilayer starts to solubilise. Lipid vesicles saturated with detergent form and coexist with mixed micelles of lipid and detergent. At stage III, the entire membrane solubilises, and only mixed micelles exist (Csucs and Ramsden 1998; Helenius and Simons 1975).

Osteoblast were cultured on the waveguides and imaged alive with time laps WEFF microscopy. At a certain time Triton X-100 was added to the medium to start solubilisation. Fig.6 shows the normalized integrated intensity of the WEFF fluorescence signal of three example cells imaged with time.

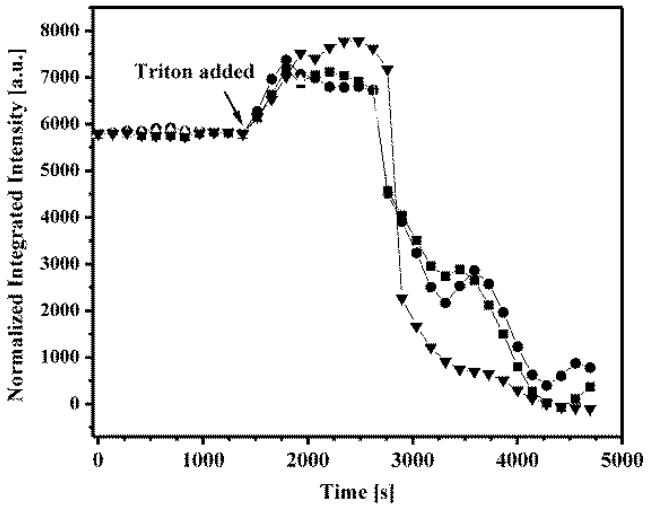

Figure 6: Normalized, integrated intensities of three cells versus time. Triton X-100 (0.013 w/w%) was added where indicated by the arrow.

In the absence of detergent, the integrated intensities are constant indicating negligible photo bleaching. In the presence of the detergent, three reproducible kinetic stages were found: i) an increase in fluorescence intensity, ii) a plateau, and iii) a decrease in intensity. Therefore, a comparison to or an adaption of the established three-stage model is possible. In stage I, the membrane takes up detergent and the concentration of detergent rises in the plasma membrane. The integrated fluorescence intensity increases due to suppression of fluorophore quenching by dilution of the dye with detergent (Silvius 1992) in the cell membrane. In this stage, solubilisation does not occur. According to the model, stage I ends when the membrane becomes saturated with detergent. The end of stage I is seen in Fig.6 when the intensity increase ends and the plateau starts.

In stage II of artificial membrane solubilisation, the detergent-saturated lipid bilayer undergoes a structural transition and converts partially into lipid-detergent mixed micelles; however, these micelles are not yet mobile, but still incorporated in the membrane. Therefore, stage II is seen in our data as the plateau in which intensity remains constant as the dye is not leaving the evanescent field. At this time, the dye is still located either in the membrane or in formed micelles in unquenched conditions mixed with detergent.

During stage III, the micelles become mobile and leave the evanescent field, leading to a decrease in integrated intensity. Individual micelles are too small to be seen with the WEFF microscope.

By changing the Triton X-100 concentration the duration of all three phases changed: the higher the detergent concentration the quicker the solubilisation stages (Hassanzadeh et al, 2012).

WEFF microscopy confirmed that living osteoblasts are solubilized in the same way as model membranes.

7. Kinetic Response of Osteoblasts to Trypsin

Trypsin is a serine protease and cleaves peptide chains. Therefore, trypsin is used in laboratories to cleave proteins bonding the cultured cells to the dish, so that the cells can be suspended in fresh solution and transferred to fresh dishes.

Healthy osteoblast cells were grown directly on the waveguide and monitored with time laps WEFF microscopy. Trypsin was used at 0.05 % and 0.02 % concentration. Upon addition of 0.05 % trypsin, the cells were lifted very fast and only individual focal adhesions could be imaged. However, with the lower concentration changes in cell morphology could be observed, such as cell retraction.

The quick disappearance of an individual adhesion point at the high trypsin concentration was examined. The focal adhesion point had the appearance of a bright circular dot. A series of images were taken with time and analyzed. Fig.7 depicts the kinetic behaviour of the adhesion point's disappearance, with respect of its integral intensity and size. Clearly both the size and the integral intensity of this individual focal adhesion point decreased in an S-shaped curve and provided basically identical kinetic information about the detachment of the cell.

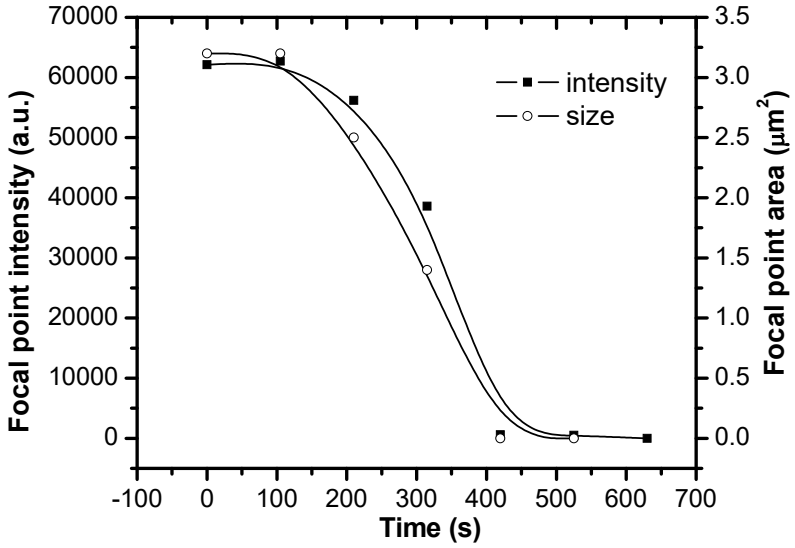

Figure 7: The impact of a 0.05 % trypsin containing medium on an individual focal adhesion: intensity and size decrease with time. The lines are guides to the eye.

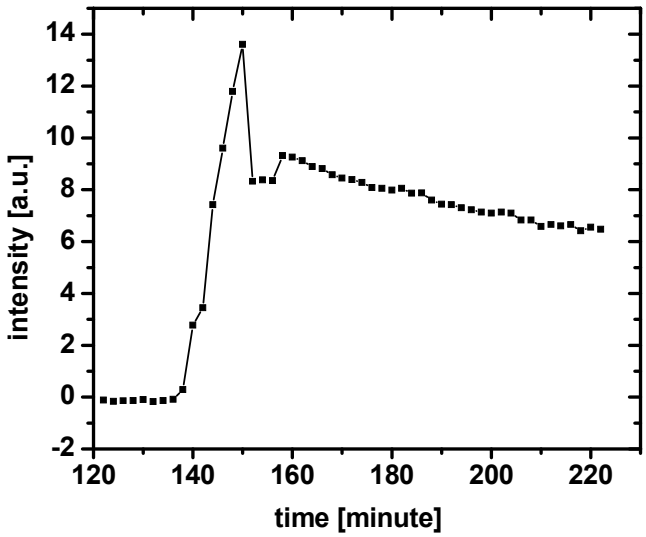

Figure 8: Integrated, intensity of 5 individual re-appearing adhesion points after exchanging a trypsin-containing medium at t = 0 to a trypsin-free medium.

A sample was treated with 0.02 % trypsin. The cells have shown cell retraction, and detached from the surface, leaving a black feature less evanescent image. After the trypsin treatment the medium was exchanged carefully to a trypsin-free environment. The imaging was continued. The osteoblasts, still alive, re-synthesise new adhesion proteins for the formation of new adhesion points. The kinetics of the adhesion process, unit the cell population died at around 150 min and lost adhesion again, is depicted in Fig.8.

8. Bacteria Sterilization

Studies on the attachment of bacteria onto surfaces using WEFS microscopy detection is a quick method for investigations regarding bacterial sterilization treatment (Nahar et al. 2014). We hypothesized that non-potent, sterilized cells do not attach to surfaces and do not form microcolonies. Therefore, we have treated identical bacteria sample batches with different UV doses (2, 4, 8, 14, 20 and 30 mJ/cm^2). After the UV illumination the viability was measured. The UV illumination did not result in bacterial death. As a control, one sample was left without UV treatment. All bacteria illuminated with different UV doses and the control were cultured identically and examined using WEFS microscopy after 24 h. Fig.9 shows a series of WEFS and bright field images of the control and UV treated bacteria.

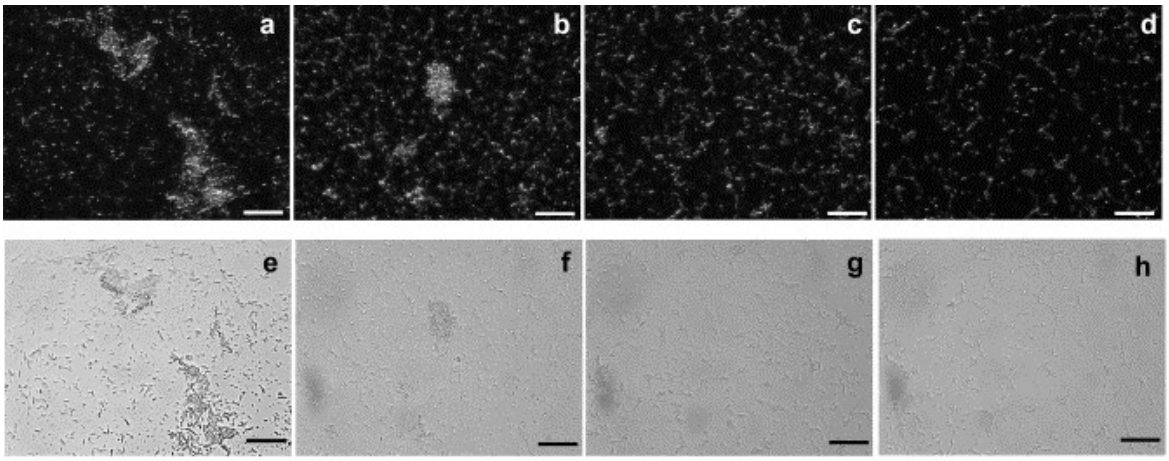

Figure 9: WEFS and bright field microscopy images of UV illuminated, sterilized bacteria after 24 h of culturing: a) and e) control: 0 mJ/cm^2), b) and f) 8 mJ/cm^2, c) and g) 20 mJ/cm^2, d) and h) 30 mJ/cm^2. The scale bar is 50 µm.

The relative signal attributed to attached colonies and individual bacteria on the waveguide surface decreased as exposure to UV illumination was increased (Fig.9). It is significant to note that the highest dose of 30 mJ/cm^2 was not sufficient to completely prevent bacterial attachment. Both WEFS and bright field microscopy demonstrated that the highest dose resulted in the attachment of primarily individual bacteria, demonstrating that while attachment still occurred with increasing UV-dose, microcolony formation was prevented.

In order to yield quantitative data, a Matlab program was written to investigate the intensity distribution of each WEFS image and to calculate the percentage of area (i.e., pixels with signals above the defined threshold) occupied by bacteria (i.e., individual cells and cells comprising distinct colonies). Fig.10 shows the percentage of area on a sample occupied by bacteria versus the applied UV dose. Although the percentage of surface area with attached bacteria was decreasing exponentially, it did not reach zero. Bacteria were still attached to the waveguide surface despite the UV treatment. A “safe”-dose can be extrapolated by the data.

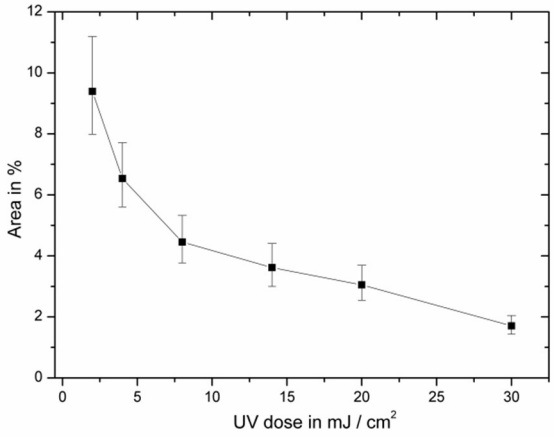

Figure 10: Percentage of occupied area of bacteria versus applied UV dose. The line is a guide to the eye only.

9. Cell Granularity and Adhesions

Fixed osteoblasts were imaged with WEFS microscopy. Fig.11 shows a bright field image of a single osteoblast and the corresponding WEFS image. In the WEFS image the nucleus can be located: it is the dark area in the cell center. In addition, the granular structures in the cell body and the adhesion sites at the cell outline were visible. Fig.11 indicates with the arrow the propagation direction of the waveguide mode. The cell's boundary first hit by the propagating light was shown very clear and with many adhesions points. The other three outer lines depict the adhesion points but not the complete cell boundary. At this chosen integration time the WEFS image depicts adhesions due to the evanescent illumination and the cell granularity due to 3D scattering of the waveguide.

Cell-substrate adhesions could be distinguished from scattering centers located further away from the substrate, the granularity of the cell, by varying the integration time. This is shown in Fig. 12.

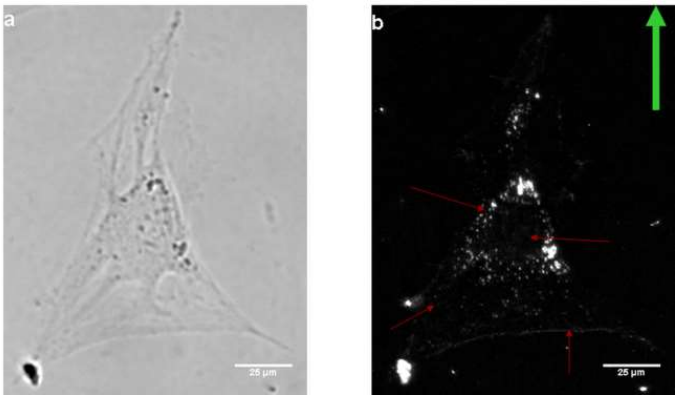

Figure 11: a) Bright field image and b) WEFS image of an osteoblast taken with an exposure time 3000 ms. The green arrow indicates the direction of light propagation. The scale bars are 25 µm.

With a very short integration time only a few spots appeared on the image in the areas where the cell was well spread. These spots are the cell's adhesions within the evanescent field. With increasing integration time, more and more features appeared, such as the cell nucleus area, the cells boundary and the cell granularity. These experiments showed that not necessarily fluorescence staining was needed for imaging focal adhesions and hence getting some cell-substratum interaction measures. As in WEFF microscopy larger integration times lead to 3D information of the cell. Further detailed analysis, e.g. whether WEFS data are comparable with flow cytometry (scattering mode), need to be done.

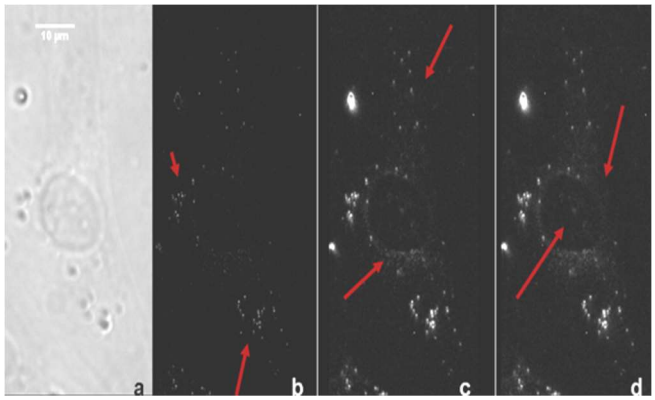

Figure 11: a) Bright field image of a single osteoblast and b)-d) corresponding WEFS images with integration times of 500 ms, 1000 ms and 1500 ms, respectively. The arrows point to the features mentioned in the text: b) adhesions, c) granularity and cell boundary, and d) nucleus and cell boundary.

10. Imaging with WEFF/WEFS Microscopy

For evanescent imaging with WEFF and WEFS microscopy on the same sample, osteoblast cells were fixed and stained. The aim was to determine the information differences in the images taken with the various evanescent microscopy forms at identical samples and integration times. It is possible to image a stained object with WEFF microscopy implementing the long pass filter to block excitation light, with WFFS/WEFS combination microscopy by collecting both scattered excitation light and fluorescence photons, and with WEFS microscopy applying a short pass filter blocking the fluorescent emission wavelengths. Fig.12 shows a series of images of a single osteoblast taken with bright field, WEFF, WEFF/WEFS and WEFS microscopy.

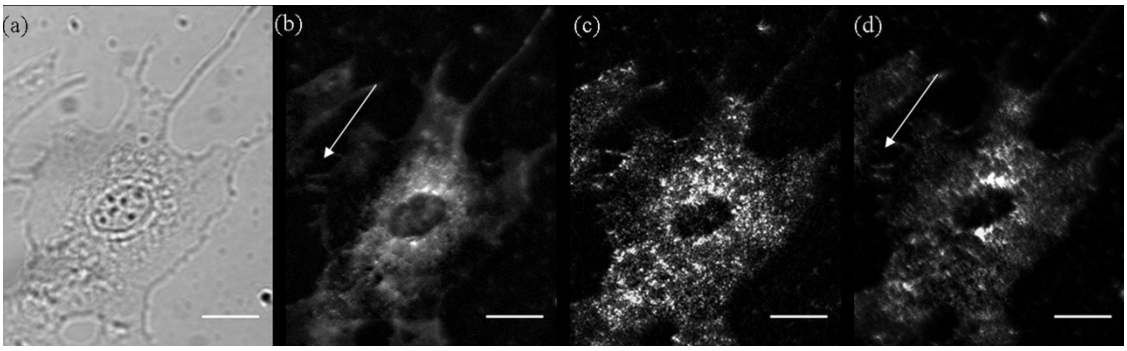

Figure 12: Osteoblast imaged with a TM mode and 6000 ms integration time: a) bright field image, b) image captured with WEFF microscopy with a 560 nm long pass filter blocking excitation light of 543 nm, c) WEFF/WEFS image captured without filters; hence both scattered and emission photons of the dye form the image, and d) image captured with WEFS microscopy with a 550 nm short pass filter blocking the fluorescence. The arrows indicate where the cell is touching an adjacent cell. Scale bars represent 20 µm.

Fig.12a shows the bright field microscopy image of a single osteoblast cell. The nucleus, and the outline of the cell were clearly visible in this image. To confirm the visualization of the entire cell with both WEFF and WEFS methods, an integration time of 6000 ms was used. The WEFF microscopy image is shown in Fig.12b. Both the cell outline and cell body was distinctly visible in the WEFF image. The nucleus appeared black with some structure in it. The cell body was distinguishable from the other parts of the cell because of the presence of many densely packed bright spots around the nucleus. The outline of the cell which is actually the spread region of the cell was less bright than the rest of the cell but still unmistakable as it was identical to the bright field image of Fig.12a. The white arrow in this image refers to the regions where the cell is touching an adjacent cell. The waveguide implemented here has an evanescent field of 100 nm. Only the close contact regions of the cell should be visible in a "real" WEFF image. But due to the high integration time, the entire cell became visible as an epi-fluorescence image where parts of the cells located far away from the surface could also be seen. Close contact regions and focal adhesions are not possible to visualize with this types of WEFF imaging strategy.

Fig.12c shows the cell captured with no filters in WEFFS/WEFS combination mode. As a result, the scattered photons and the photons from the dye emission are forming the image. Although the cell outline was visible and nucleus distinguishable, there was too much intensity present in the entire cell making it impossible to distinguish the spread region of the cell and the cell body. Also the granularity was not visible as expected (Fig.11).

Fig.12d, was captured with pure WEFS microscopy employing a 550 nm short pass filter blocking the fluorescence. This image showed the outline of the cells and the nucleus, but no clear distinguishing between the spread region of the cell and the cell body was possible. The links to the touching neighbor cell indicated by an arrow, were less prominent compared to the epi-fluorescence WEFF microscopy image. The granularity was distinctively different from the images of the cells which were not stained (Fig.11).

From these studies it became clear that both methods have their individual optimum microscopy settings for achieving informative images. The amount of scattered light increased when a cell is stained and does not necessary deliver the same information about granularity as an unstained cell. Unresolved dye might act as additional scattering centers delivering artefacts. For an informative comparison of WEFF and WEFS images two sample sets should be prepared and imaged with individual optimized conditions (microscope settings and sample preparation).

11. All-Polymer-Waveguide-Chips

In order to allow WEFF and WEFS microscopy to be used by the interested communities, typically biophysics, biology, biochemistry and medical laboratories, but also for coating engineering (aging studies, homogeneity studies, anti-microbial tests, etc.) the waveguide chips need to be (commercially) available and at a reasonable cost. Mass production is the only way to accomplish this. An all-polymer-waveguide-chip with an imprinted coupling grating is one way to achieve this goal.

We have designed an all-polymer-waveguide chip on the basis of a PMMA substrate. The imprinting was performed into the PMMA with a home-fabricated silicon stamp, and in a subsequent step a polystyrene waveguide was spin coated on top.

Fig.13 shows an SEM image of an imprinted grating with a periodicity of 670 nm and a depth of 200 nm.

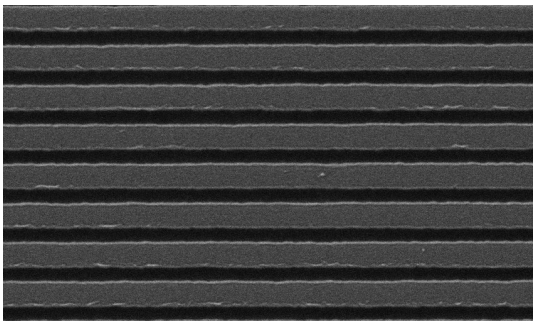

Figure 13: SEM image of a PMMA imprinted coupling grating. The periodicity is 670 nm.

First experiments with the all-polymer-waveguide-chips have produced promising WEFF imaging results (Fig.14). The WEFF image of the HeLa cell on the all-polymer-waveguide-chip does still look like an epi-fluorescence image. Also the distinct spotty or dotty pattern due to the adhesions at the end of the filopodia and at the outer rim of the cell are still missing. The polymer chips still suffer from too many scattered photons (Sharon and Mittler, 2016) due to too many imperfections in the waveguide. The waveguide spin coating conditions need to be improved (dust free and with a homogeneous thickness throughout the sample). In addition, development towards mass produced chips is necessary. The grating of Fig.11 and the all-polymer-waveguide-chip of Fig.14 were fabricated by imprinting one grating into one PMMA substrate. The imprinting and waveguide spinning procedure needs to be scaled up to fabricate 16, 25, 36 or more chips in parallel on one substrate with one imprinting procedure and a subsequent high quality spin coating process and subsequent separation of the individual chips.

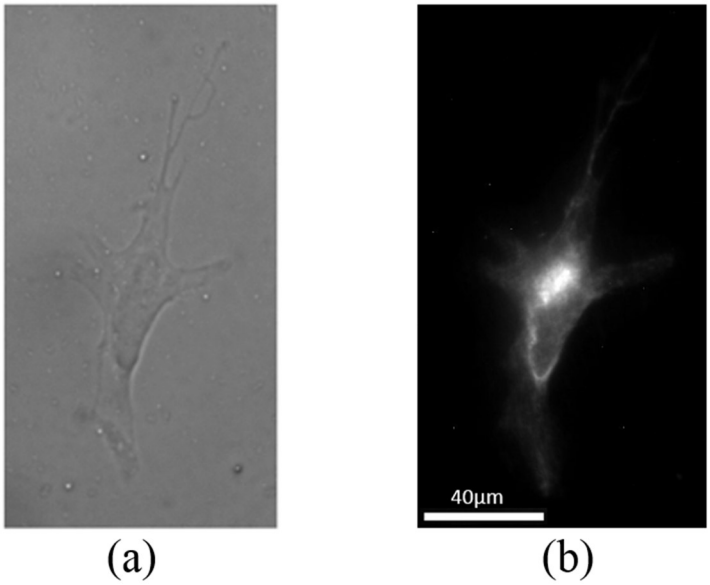

Figure 14: All-polymer-waveguide-chip: a) Bright field image and b) WEFF image of a HeLa cell stained with DiO.

12. Conclusions and Outlook

A simple method to perform TIR and TIRF microscopy with a conventional inverted optical microscope by implementing an optical slab waveguide as the illumination source was discussed as well as the suit of advantages a confined beam in a waveguide offers in comparison to a standard TIR(F) microscope.

Both WEFF and WEFS microscopies were applied to a variety of biophysical questions: simple imaging of adhesions, quantitative investigations such as dye distance mapping and analyzing kinetic phenomena. A critical analysis of images taken in a WEFF/WEFS combination found that the combination is not recommendable. Each method should be used on samples especially prepared and with the optimum individual microscopy and image acquisition conditions.

In order to make the technology available for an interested scientific community, the availability of the waveguide-chip is essential. Therefore, a methodology for the fabrication of a mass produced, cost-effective waveguide-chip based on polymers only was developed and tested. In the future, the all-glass-chips should come with a surface functionalization allowing reusability. Time laps distance mapping is not possible yet, but planned.

Various types of interface and surface related biophysical and biological questions can be addressed with WEFF/S microscopy. They carry in addition the opportunity of an implementation in senor technology. Various options have been published already (Agnarsson et al. 2010; Agnarsson et al. 2015).

There is a huge opportunity to also use WEFF/S for advanced measurements. The WEFF microscope can be simultaneously operated by propagating modes at different wavelength or directions for any kind of pump probe or resonance experiment, or a sensing scheme based on a Förster transfer in a dye upon binding of an analyte. Pulsed laser operation is another option. The scattering microscopy is responsive to any changes in the size or the refractive index (density) of the scattering entity within the evanescent field. The monitoring sensitivity of surface recognition reactions could easily be enhanced by increasing the scattering power by a gold nanoparticle (Klein 2008) or by increasing the size of a scattering entity due to the binding (Agnarsson et al. 2015).

Silane chemistry will allow to tune the waveguide's surface functionalization, both for all-glass and all-polymer-chips. Hydroxyl groups can easily be produced by oxygen plasma or UV ozone treatment for further functionalization (Kandeepan et al. 2015).

Acknowledgements

Many co-workers, students, PDFs and colleagues are thanked for their contribution in the past, the present and the future for developing and applying WEFF and WEFS microscopy: Frank Thoma, Uwe Langbein, John J. Armitage, Huge Trembley, Michael Nietsche, Abdollah Hassanzadeh, Elisabeth Pruski, Jeffrey S. Dixon, Stephen Sims, Rebbeca Stuchburry, Sabiha Hacibekiroglu, Daniel Imruck, Christopher Halfpap, Michael Morawitz, Qamrun Nahar, Darryl K. Knight, Susanne Armstrong, Jeremia Shuster, Frederik Fleisser, Mihaela Stefan, Kibret Mequanint, Beth Gillies, Rene Harrison, Gordon Southam, Cheryle Seguin, Hong Hong Chen, Donglin Bai, Douglas Hamilton and Rony Sharon.

References

Abercrombie, M, Heaysman, J.E., and Pegrum, S.M., 1971, Exp. Cell Res. **67**, 359 – 367.

Agnarsson, B., Ingthorsson, S., Gudjonsson, T., and Leosson, K., 2009, Optics Express **17**, 5075-5082.

Agnarsson, B., Halldorsson, J., Arnfinnsdottir, N., Ingthorsson, S., Gudjonsson, T., and Leosson, K., 2010, Microelectronic Engineering **87**, 56–61.

Agnarsson, B., Jonsdottir, A.B., Arnfinnsdottir, N.B., and Leosson, K., 2011, Optics Express **19**, 22929 - 22935.

Agnarsson,B., Lundgren,A., Gunnarsson, A., Rabe,M., Kunze,A., Mapar,M., Simonsson, L., Bally,M., Zhdanov, V.P., and Höök, F., 2015, ACS Nanao **9**, 11849–11862.

Atilgan, E., and Ovryn, B., 2009, Current Pharmaceutical Biotechnology **10**, 508 – 514.

Bauereiss, A., Welzel, O., Jung, Grosse-Holz, S. Lelental, N., Lewczuk, P., Wenzel, E.M., Kornhuber, J. , and Groemer, T. W., 2015, Traffic **16**, 655-675.

Berney, M., Hammes, F., Bosshard, F., Weilenmann, H.-U., and Egli, T., 2007, Applied and Environmental Microbiology **73**, 3283–3290.

Braun, B., and Fromherz, P., 1997, Applied Physics A-Materials Science & Processing **65**, 341 – 348.

Burmeister, J.S., Truskey, G.A., and Reichert, W.M., 1994, Journal of Microscopy-Oxford **173**, 39 – 51.

Burmeister, J.S., Olivier, L.A., Reichert, W.M., and Truskey, G.A., 1998, Biomaterials **19**, 307 – 325.

Burmeister, J.S., Truskey, G.A., Yarbough, J.L., and Reichert, W.M., 1994, Biotechnological Progress **10**, 26-31.

Byrne, G. D., Pitter, M.C., Zhang, J., Falcone, F.H., Stolnik, S., and Somekh, M.G., 2008, Journal of Microscopy, 231, 168-179.

Chen, W.T., and Singer, S.J., 1982, Journal of Cell Biology **95**, 205 - 222.

Christianson, G.E., 2004, in Molecular Adhesion and Its Applications, The Sticky Universe, ed. Kevin Kendal, 275-303.

Cooper, I.R., Meikle, S.T., Standen, G., Hanlon, G.W., and Santin, M., 2009, J. Microbiol. Meth. **78**, 40-44.

Csucs, G., and Ramsden, J.J., 1998, Biochimica et Biophysica Acta **1369**, 304–308.

Durbeej, B., and Eriksson, L.A., 2002, Journal of Photochemistry and Photobiology A: Chemistry **152**, 95–10.

Fleissner, F., Morawitz, M., Dixon, S.J., Langbein, U., und Mittler, S., 2014, Journal of Biophotonics 1-12.

Giebel, K.F., Bechinger, C., Herminghaus, S., Riedel, M., Leiderer, P., Weiland, U., and Bastmeyer, M., 1999, Biophysical Journal **76**, 509 – 516.

Grandin, H.M., Städler, B., Textor, M., and Vörös, J., 2006, Biosensensors and Bioelectronics **21**, 1476-1482.

Halfpap, C., Morawitz, M., Peter, A., Detrez, N., Mittler, S., and Langbein, U., 2012, DGaO Proceedings, 0287-2012.

Hassanzadeh, A., Nitsche, M., Mittler, S., Armstrong, S.,J., Dixon, J., and Langbein, U., (2008) Applied Physics Letters **92**, 233503.

Hassanzadeh, A., Armstrong, S., Dixon, S.J., and Mittler, S., 2009, Applied Physics Letters 94, 033503.

Hassanzadeh, A., Nitsche, M., Armstrong, S., Nabavi, N., Harrison, R., Dixon, S.J., Langbein, U., and Mittler, S., 2010, Biomedical Optics 15 036018-1 - 036018-7.
Hassanzadeh, A., and Mittler, S., 2011, Optical Engineering **50,** 071103.
Hassanzadeh, A., Kan Ma, H., Dixon, S.J., and Mittler, S., 2012, Biomedical Optics **17**, 076025 1-7.
Hedrick, R.P., Petri, B., McDowell, T.S., Mukkatira, K., and Sealey, L.J., 2007, Diseases of Aquatic Organisms **74**, 113-118.
Helenius, A., and Simons, K., 1975, Biochimica et Biophysica Acta **415**, 29–79.
Hetrick, E.M., and Schoenfisch, M.H., 2006, Chem. Soc. Rev. **35**, 780-789.
Horvath, R., Vörös, J., Graf, R., Fricsovszky, G., Textor, M., Lindvold, L.R., Spencer, N.D., and Papp, E., 2001, Applied Physics B **72**, 441-447.
Horvath, R., Pedersen, H.C., Skivesen, N., Selmeczi, D., and Larsen, N.B., 2005, Applied Physics Letters **86**, 071101.
Hug, T.S., Prenosil, J.E., and Morbidelli, M., 2001, Biosensors & Bioelectronics **16**, 865–874.
Hug, T.S., Prenosil, J.E., Maier, P., and Morbidelli, M., 2002, Biotechnology and Bioengineering **80**, 213-221.
Hug, T.S., Prenosil, J.E., Maier, P., and Morbidelli, M., 2002, Biotechnol. Prog. **18**, 1408-1413.
Kandeepna, S., Paquette, J.A., Gilroy, J.B., and Mittler, S., 2015, CVD, **21**, 275–280.
Keshmiri, H., Agnarsson, B., and Leósson, K., 2011, SPIE Vol. 8090, 80900D1-6.
Klein, A., Diploma Thesis, RheinMain University, Rüsseleheim, Germany, 2008.
Kuo, J., Asce, M., Chen, C.-L., and Nellor, M., 2003, Journal of Environmental Engineering **129** 774-779.
Leosson, K., and Agnarsson, B., 2012, Micromachines **3**, 114-125.
Liu, X., Welf, E.S., and Haugh, J.M., 2015, Journal of the Royal Society, Interface **12**, 20141412 (1-11).
Madkour., A.E., and Tew, G.N., 2008, Polym. Intl. **57**, 6.
Madkour, A.E., Dabkowski, J.M., Nusslein, K., and Tew, G.N., 2009, Langmuir **25**, 1060-1067.
Mazhorova, A., Markov, A., Ng, A., Chinnappan, R., Skorobogata, O., Zourob, M., and Skorobogatiy, M., 20012, Opt. Express **20**, 5344-5355.
Lanier, L.L., and Warner, N.L., 1981, Journal of Immunological Methods **47**, 25-30.
Lichtenberg, D., Robson, J., and Dennis, E.A., 1985, Biochimica et Biophysica Acta **821**, 470–478.
Nahar, Q., Fleissner, F., Shuster, J., Morawitz, M., Halfpap, C., Stefan, M., Southam, G., Langbein, U., and Mittler, S., 2014, Journal of Biophotonics, 7, 542–551.
Niu, X.F., Wang, Y.L., Luo, Y.L., Xin, J., and Li, Y.G. 2005. Journal of Materials Science & Technology **21**, 571- 576.
Ngassam, V.N., Howland, M.C., Sapuri-Butti, A., Rosidi, N., and Parikh, A.N., 2012., Soft Matter **8,** 3734-3738.
Oliver, J.D., 2005, J. Microbiol. **43**, 93-100.
Pera, N.P., Kouki, A., Haataja, S., Branderhorst, H.M., Liskamp, R.M.J., Visser, G.M., Finne, J., and Pieters, R.J., 2010, Org. Biomol. Chem. **8**, 2425-2429.
Pires, L., Sachsenheimer, K., Kleintschek, T., Waldbaur, A., Schwartz,T., and Rapp, B.E., 2013, Biosensors and Biolectronics **47**, 157-163.
Pizarro-Cerda, J., and Cossart, P., 2006, Cell **124**, 715-725.

Sapsford, K.E., and Shiver-Lake, L.C., 2008, in Zourob, M., Elwary, S., and Turner, A.P.F. eds, Principles of Bacterial Detection: Biosensors, Recognition Receptors and Microsystems. Springer, 109-123.
Schmidt, M., Hourfar, M.K., Nicol, S.-B., Wahl, A., Heck, J., Weis, C., Tonn, T., Spengler, H.-P., Montag, T., Seifried, E., and Roth, W.K., 2006, Transfusion **46**, 1367-1373.
Sharon R., and Mittler, S., 2016, Journal of Biomedical Optics, submitted.
Silvius, J. R.,1992, Annual Review of Biophysics and Biomolecular Structure **21**, 323-348.
Smith, L.V., Tamm, L.K., and Ford, R.M., 2002, Langmuir. **18**, 5247-5255.
Smit, J.W., Meijer, C.J.L.M., Decay, F., and Feltkamp, T.M., 1974, Journal of Immunological Methods **6**, 93-98.
Su, J.-W., Hsu, W.-C., Tjiu, J.-W., Chiang, C.-P., Huang, C.-W., and Sunga, K.-B., 2014, Journal of Biomedical Optics **19**, 075007.
Stamm, W.E., 1978, *Annals of International Medicine* **89**, 764-769.
Storrie, H., Guler, M.O., Abu-Amara, S.N., Volberg, T., Rao, M., Geiger, B., and Stupp, S.I., 2007, Biomaterials **28**, 4608 - 4618.
Tawil, N., Wilson, E., and Carbonetto, S., 1993, Journal of Cell Biology **120**, 261 – 271.
Taylor, A.D., Ladd, J., Homolas, J., and Jang, S., 2008, in Zourob, M., Elwary, S., Turner, A., eds., Principles of Bacterial Detection: Biosensors, Recognition Receptors and Microsystems XXXII (Springer) 83-108.
Thoma, F., Langbein, U., and Mittler-Neher, S., 1997, Optics Communications **134**, 16-20 (1997).
Thoma, F., Armitage, J.J., Trembley, H., Menges, B., Langbein, U., and Mittler-Neher, S., 1998, Proceedings of SPIE **3414,** 242-249.
Vasilev, K., Cook, J., and Griesser, H.J., 2009, Expert Rev. Med. Devices **6**, 553-567.
Verschueren, H., 1984, J Cell Sci **75**, 279 – 301.
Vigeant, M.A.S., Wagner, M., Tamm, L.K., and Ford, R.M., 2001, Langmuir **17**, 2235-2242.
Truskey, G.A., Burmeister, J.S. Grapa, E., and Reichert, W.M., 1992, Journal of Cell Science 103, 491-499.
Zourob, M., Mohr, S., Brown, B.J.T., Fielden, P.F., McDonnell, M.B., and Goddard, N.J., 2005, Biosensors and Bioelectronics **21**, 293-302.